Spatial Dynamic Analysis of A Mangrove Patch Based On Unmanned Aerial Vehicle: A Case Study In Pear Bay In Guangxi, China

Xin Lin (Lxin_95@126.com)
forest inventory and planning institute of Guangxi https://orcid.org/0000-0003-3625-6051
Chungan Li
Guangxi University
Mei Zhou
Guangxi University
Wenhai Liang
French National Forestry Inventory: Institut national de l'information geographique et forestiere
Biao Li
Forest Inventory and planning institute of Guangxi

Research Article

Keywords: Mangrove, Spatial dynamic analysis, UAV, CHM

Posted Date: July 23rd, 2021

DOI: https://doi.org/10.21203/rs.3.rs-425731/v2

Abstract

This study investigated the short-term spatial variability of an mangrove patch, located in the Pearl Bay in Guangxi, China. Unmanned aerial vehicle (UAV) imagery covering the period from March 2015 to October 2017 were used and the following models were developed: two annual ultra-high resolution spatial resolution digital orthophoto maps (DOMs), two digital elevation models (DEMs), two digital surface models (DSMs), two canopy height models (CHMs), and a canopy height difference model (d-CHM). Using these models, the spatial dynamics of the extent and canopy height of the patch were analyzed. The resolution of the DOMs was 0.1 m, with an average geometrical error of 0.17 m and a maximum error of 0.44 m. The resolutions of DEMs, DSMs, CHMs, d-CHM were all 1 m. The average elevation errors of CHM in 2015 and 2017 were 0.002 m and -0.001 m, respectively, with maximum absolute errors of 0.034 m and 0.030 m, respectively. The average elevation error of d-CHM was -0.003 m and the maximum absolute error was 0.036 m, and the data quality were rated as good. From 2015 to 2017, the area of the mangrove patch increased from 8.16 ha to 8.79 ha, with an average annual increase of 3.7%. Specifically, the areas of expansion, shrinkage, and maximum seaward expansion were 6356 m^2, 19 m^2, and 24 m, respectively. The driving factor for the variability was natural processes. Stand canopy height exhibited a particular trend of decrease from northwest to southeast (horizontal; parallel to the seawall) and from the land to the sea (vertically; perpendicular to the seawall). From 2015 to 2017, 88.2% of the patch area showed increased canopy height, with an average increase of 0.78 m and a maximum increase of 3.2 m. In contrast, 11.8% of the patch area showed decreased canopy height with a maximum decrease of 3.1 m. The main reason for the decrease in canopy height was the death of trees caused by serious insect plagues. On the other hand, the reason for the increase in height could be attributed to the natural growth of mangrove trees, but further studies are required to verify the cause. UAV remote sensing has an incomparable advantage over traditional methods in that it provides extremely detailed and highly accurate information for in-depth study of the spatial evolution of mangrove patches, which would significantly contribute towards the protection and management of mangroves.

Introduction

Mangrove forests are intertidal forests that exist in estuaries, river banks, and lagoons in both tropical and subtropical regions, and they are one of the most productive ecosystems (FAO 2007; Walters et al. 2008; Nagalakshmi 2017). Mangrove forests provide a number of essential supplies such as wood, non-wood products, and marine food for residents in nearby communities (Palacios and Cantera 2017; Benzeev et al. 2017).As the basic food source for a large number of marine animals, mangrove forests also directly affect the health and function of the marine food chain (Saenger et al. 1983). In addition, mangrove forests provide habitats, breeding sites, and breeding grounds for numerous marine and terrestrial animals. By intercepting land runoff and sediment, mangroves help in protecting coral reefs, seagrass beds, and waterways. Mangrove forests also contribute to the prevention and reduction of coastal erosion. Furthermore, mangroves serve as significant revetments against strong waves by reducing the speed and intensity of strong waves and promoting siltation, thus playing a central role in the reduction of hurricane erosion and impacts of storm surges (Doughty et al. 2016). The 2004 Indian Ocean tsunami proved the importance of protecting mangroves and coastal forests (Teh et al. 2009; Yanagisawa et al. 2009, 2010). Given their significance, mangrove forests are an ideal research subject in the field of biodiversity, ecosystems, aquatic products, and global change. The

mangrove ecosystem also supports aquaculture, including open-estuary aquaculture (such as oysters and mussels) and pond culture (FAO 2007).

The mangrove ecosystem has been facing serious threats from sea level rise, climate change, and human activities such as aquaculture, land reclamation, urbanization, infrastructure construction, and pollution (UNEP 2014, Lovelock et al. 2015). With continued shrinkage, mangrove forests are experiencing fragmentation of habitats and their long-term survival is being threatened; moreover, their fundamental ecological impacts have declined. Scholars believe that the ecological services and benefits of mangrove forests could disappear in the next 100 years (Duke et al. 2007). Therefore, there is an urgent need to strengthen the protection, conservation, and ecological restoration of mangroves.

Mangrove ecosystems are extremely sensitive to changes in coastal environments and have the potential to reflect environmental changes (Blasco et a1. 1996). Consequently, the possible responses of mangrove communities to coastal environmental changes, including sea level rise and climate change, have attracted the interest of many scholars. In most cases, changes in mangrove forests are attributable to natural processes. For instance, the expansion and regression of mangrove forests is a response to deposition and erosion. Changes in mangrove forests are also a very delicate process, such as the response of mangroves to sea level rise. To fully understand the response of mangroves to environmental changes, the monitoring of several factors, such as the extent, structure, and plant composition of mangroves, is necessary. In this respect, it is particularly important to establish baseline data for mangroves (Lucas et a1. 2002). Furthermore, investigating the changes in the extent and structure of natural mangroves at the local level and patch level is helpful to understand the establishment, expansion and driving factors of mangroves in the natural state, and has important reference value for mangrove artificial afforestation and ecological restoration.

Considering the inaccessibility of the tidal flat environment, remote sensing technology, which offers wide coverage and objectivity, is widely used for mangrove monitoring and mapping. High spatial resolution remote sensing images, such as those from SPOT5, IKONOS, QuickBird, WorldView, and aerial photography, are often used to monitor the spatial distribution and analyze dynamic changes of mangroves at the regional and local levels (Everitt et al. l991, 2008; Dale et al. 1996; Manson et al. 2001, 2003; Dahdouh-Guebas et al. 2002, 2004; Sulong et al. 2002; Fromard et a1. 2004; Kovacs et al. 2004, 2005; Rodriguez et al. 2004; Wang et a1. 2004; Benfield et a1. 2005; Kanniah et a1. 2007; Olwig et a1. 2007; Proisy et a1., 2007; Neukermans et al. 2008; Saleh 2007; Lee and Yeh 2009; Kux et al. 2012; Heenkenda et al. 2014; Wang et al. 2014; Liu et a1. 2017; Rizki et a1. 2017). Some scholars used interferometric radar, spaceborne and airborne LiDAR and stereo aerial photography to study the spatial structure (such as tree height) and function (such as biomass and carbon sink) of mangroves, and achieved good results (Simard et al. 2006, 2008; Mitchell et al. 2007; Fatoyinbo and Simard 2013; Lee and Fatoyinbo 2015; Aslan et al. 2016). Although high-resolution optical remote sensing data can be used to accurately map the distribution of mangroves, they do not support three-dimensional mapping. Airborne LiDAR data can be used in the accurate determination of mangrove distribution, two-dimensional and three-dimensional mapping of canopy, and estimation of forest biomass. However, the acquisition of LiDAR data is extremely costly. With technological developments, unmanned aerial vehicle (UAV) remote sensing has facilitated the dynamic monitoring of local-scale mangrove forests with extremely high spatial resolution and elastic revisit frequency at low cost (Tian et a1. 2017). UAV laser radar remote sensing supports the acquisition of high-precision, three-dimensional ground and vegetation information, including canopy height, canopy

coverage, leaf area index (LAI), and aboveground biomass (Guo et al. 2017; Tian et al. 2017; Cao et al. 2018; Otero et al. 2018).

In this study, a mangrove patch with an area of 8.8 ha was selected as the research subject, and low-altitude UAV remote sensing was applied to monitor the patch extent and dynamic canopy height. The goal of this research is to precisely understand the mechanics, processes, and driving factors of mangrove patch dynamics in the short term, as well as the canopy height distribution pattern and its evolution. For this purpose, digital orthophoto maps (DOMs), digital elevation models (DEMs), digital surface models (DSMs), crown height models (CHMs), and dynamic crown height mode1 (d-CHM) were developed using data from UAV remote sensing. Combined with field measurement data, the potential of three-dimensional mapping of mangroves using UAV remote sensing was analyzed. UAV remote sensing provides an accurate, reliable, informative, intuitive, cost-efficient, and rapid method for monitoring the spatial evolution of mangroves on the patch or stand scale.

Study Site And Data Collection

Study site

The study site is a mangrove patch located in front of the Xiti seawall from Tanji Village to Wanwei Island, on the west side of the Pearl bay in Fangchenggang region in Guangxi, China (Fig. 1). The patch is a community of *Avicennia marina*, with a small population of *Aegiceras corniculata*. This patch was formed on a bare beach in the late 1970s and early 1980s after the seawall was built in 1969; its area was 1.62 ha in 1989 and expanded to 8.16 ha in 2015 (Li and Zhou 2017).

The Pearl bay is a funnel-shaped bay with an area of 94 km^2 and a mouth width of 3.5 km. It lies adjacent to the Beilun River estuary in the west, at the border between China and Vietnam, and Fangcheng gulf in the east. It is injected by the Naso River and Huangzhu River at the top of the bay. Tides in the Pearl bay are normal diurnal tides, with an average tidal range of 2.24 m, a maximum tidal range of 5.05 m. The average wave height is 0.40–0.72 m, maximum wave height is 4.10 m, and average annual seawater salinity is 29.10‰. Most of the bottom sediments in this bay are medium–fine sands and sandy silts, along with some gravel. The annual average temperature in the Pearl bay is 22.5 ℃; the hottest month is July, during which the monthly average temperature is 28.6 ℃, and the coldest month is January, during which the monthly average temperature is 14.1 ℃. The annual average precipitation in the Pearl bay is 2200 mm (Li and Li 1993).

Data Acquisition by Unmanned Aircraft

Aircraft system and composition

In March 2015, the fixed triangle wing UAV T-EZ manufactured by Beijing Tianyu Chuangtong Technology Co., Ltd. (Creation) was used for aerial photography acquisition. The aircraft has a wingspan of 2.0 m, a length of 0.8 m, and a take-off weight of 5 kg. It was equipped with a Sony A7R full-frame camera with an effective pixel size of 42 million and a 35 mm lens. The pixel size was 4.88 micron and the image size was 7360 × 4912 pixels (Creation 2018). The UAV took off in the ejection takeoff mode, with a maximum horizontal speed of 120 km/h, cruise speed of 75 km/h, and maximum flight altitude of 5000 m.

In October 2017, the four-rotor UAV DJI Phantom 4 (Shenzhen DJI Technology Co., Ltd.) was used for aerial photography acquisition. The weight (including battery and slurry) of the aircraft was 1380 g, wheelbase was 350 mm, and maximum horizontal flying speed was 72 km/h. The maximum altitude was 6000 m, maximum flying time was approximately 28 min, and vertical hovering accuracy was ± 0.1–0.5 m, and horizontal accuracy was ± 0.3–1.5 m. The GPS/GLONASS dual-mode was used for satellite positioning and the aircraft had a relatively stable flying attitude. A three-axis stabilization system (pitch, roll, and yaw) was adopted. The range of rotation was pitch − 90°–+30°, maximum control speed was pitch − 90°/s, and angle control precision was ± 0.02°. The lens was FOV84° 20 mm (35 mm format equivalent), the f/2.8 focus was infinite, the sensor was 1 inch CMOS, the effective pixel was 12.4 million dpi, and the image size was 4000 ×3000 pixels (DJI-Innovation 2018).

Data acquisition

On March 15, 2015, the UAV flied at an altitude of 500 m for aerial photography; the overlapping on course line was 70%, side overlapping was 55%, and spatial resolution photos was 0.08 m. From October 22 to 23, 2017, the flight altitude was changed to 200 m for aerial photography; the overlapping on course line was 70%, side overlapping was 70%, and spatial resolution of photos was 0.05–0.06 m.

The UAV was used in the Guangxi Continuous Operation Reference Station Integrated Service system (Guangxi CORS) for navigation. Four spots on the ground (seawall and road) were selected and Real-Time Kinematic was used to survey their three-dimensional coordinates as ground control points.

Field investigation

On October 22, 2017, three sample lines were laid on the patch dykeward to seaward, 3–4 sample trees were selected in each sample line and the heights of a total of 10 sample trees were measured. Each sample tree was positioned using Trimble GEO EXPLORER6000XT handheld GPS.

Methods

Aerial photograph development and data accuracy test

Photo preprocessing

The Photoshop software package was used to adjust the brightness, color, and saturation of the aerial photographs to ensure consistency of the holistic color.

The Sony a7R camera is not a photogrammetric camera, and it is limited by the processing and assembly technology of its optical system. There are some issues such as aberration, angular magnification and effective diaphragm position change, non-coincidence between pupil center and main point, and eccentricity between lenses. These lead to distortion and asymmetry of the whole optical system. Hence, correction and calibration for distortion is required, for which the following processes were followed. Firstly, the focal length was adjusted to infinity, and the lens was fixed with an insulating tape. The lens focus dial was adjusted to manual mode. Then, in a high-precision three-dimensional in-door control field, several pictures were taken at multiple locations and the photographic lens was calibrated by means of parameter calculation according to

the principle of bean adjustment. After obtaining the calibration parameter table, the 10-parameter model was used to process the distortion of the photos.

Generation of DEM and DSM and DOM

The DEM, DSM, and DOM were developed using the INPHO4.0 software package, and the specific methods are as follows:

1) Photos, POS data, control point files, and camera parameters were imported into the software. After the connection points were generated by automatic matching, the relative orientation of the photos was completed, and a photo pyramid was created. Then, the connection points were automatically generated and connection points with large errors and errors were manually eliminated, and the regional network adjustment calculation and the aerial triangulation calculation were performed.

2) Interpolation automatic matching and encryption were performed using the least squares surface fitting method, and point cloud data were output.

3) The point cloud data were classified into vegetation and non-vegetation points (ground and seawall points) using the LSC (LiDAR Studio Classification) software package (Guangxi Guineng Information Engineering Co., Ltd.). Then, points that were obviously lower or higher than the ground, such as poles, wires, and insect killing lights, were separated and eliminated.

4) The least squares surface fitting method was used to build DEM with ground point cloud data, and DSM was generated from all point cloud data. The spatial resolution of DEN and DSM were both 1.0 m.

5) Through the internal and external azimuth elements and DEM, the original images were automatically digitally differentiated, and the monolithic digital orthophoto was generated. After uniform light and uniform coloring, single digital orthophoto mosaicking was performed to obtain the DOM of the study site. The spatial resolution of the DOM was 0.1 m.

Generation of CHM and d-CHM

The CHMs of the patch in 2015 and 2017 were obtained by subtracting the DEMs from the DSMs of the corresponding years. The d-CHM of the patch from 2015 to 2017 was obtained by subtracting the 2015 CHM from the 2017 CHM. The above models were tailored according to the range of study site and patch.

Data accuracy check

DOM plane accuracy: In the GIS software environment, 12 homonymous points from seawalls and culturing pond drainage structures were selected in the DOM of two years, and the plane coordinates were read. The plane distance of the same point in the two-year DOM was taken as the plane error of the two annual DOMs.

Relative elevation accuracy: In the GIS software environment, the theoretically stable elevation of hardened pavement and beach checkpoints around the patches were extracted from the DEM, DSM, and d-CHM for 2015 and 2017. For all the checkpoints, if DSM_{2015}-DEM_{2015} = 0, DEM and DSM for 2015 can be considered to have the same elevation accuracy. This test showed that the accuracy of the annual CHM elevation was highly

reliable. Similarly, for all the checkpoints, if DSM_{2017}-DEM_{2017} = 0, the elevation accuracy for 2017 can be considered to be reliable. For all checkpoints, if d-CHM = 0, the elevation accuracy of d-CHM is highly reliable.

To verify the accuracy of the height extracted from CHM, the measured height of the 10 sample trees were compared with the height extracted from CHM for 2017.

Analysis of the evolution of the distribution of mangroves

The spatial extent of the mangrove patch was analyzed using a spatial overlay method in the GIS software environment.

1) The screen vectorization method was used to visually extract the patch boundaries in 2015 and 2017, respectively. Then patch maps of the two years were obtained.

2) The polygon of the mangrove patch of the two years were converted into polylines, cutting the 2017 polygon with the 2015 polyline and cutting the 2015 polygon with the 2017 polyline. Then the polygon of the two years was overlaid on the DOM to individually determine the mechanism and driving factors of changes in patch extent (Li et al. 2012; Li 2013; Li and Dai 2015).

Dynamic Analysis of Crown Height

Using the CHM for the two years, the overall spatial pattern of tree height in the mangrove patch in 2015 and 2017 was analyzed. The spatial pattern of mangrove canopy in typical areas was analyzed by longitudinal (vertical to seawall) and horizontal (parallel to seawall) profile lines.

d-CHM was used to analyze the spatial evolution of canopy height from 2015 to 2017.

Result

Data Accuracy

Accuracy of DEM, DSM and DOM and d-CHM

DOM adjustment: The maximum errors were as follows: $|\triangle x|$=0.032 m, $|\triangle y|$=0.032 m,$|\triangle z|$=0.000 m.

The average deviation of DOM of the 12 corresponding points in the two-phase images was 0.17 m, and the maximum deviation was 0.44 m. As the deviation was considerably small, the coincidence of the two-phase DOM was satisfactory, facilitating accurate analysis of the spatial variation of the patch.

The average errors of DEM and DSM for 2015 and 2017 were 0.002 m and − 0.001 m, respectively, and the maximum absolute errors were 0.034 m and 0.030 m. This indicates that the accuracy of the CHM for the two years reached the centimeter level. In other words, the height distribution of tree canopy in 2015 and 2017 could be accurately modeled. The average error of d-CHM was − 0.003 m, and the maximum absolute error was 0.036 m, indicating that d-CHM could accurately reflect the height change of tree canopy from 2015 to 2017.

Comparison between measured height and CHM height

Comparing the height of 10 samples extracted from the CHM for 2007 with field measurement results, the average error, maximum absolute error, and standard deviation (SD) were found to be 0.07 m, 0.61 m, and 0.36 m, respectively (Table 1).

Table 1
Comparison of field measured height with modeled height for 2007

No. of tree	1	2	3	4	5	6	7	8	9	10	mean error (m)	SD (m)
Measured tree height (m)	3.14	5.26	4.32	4.30	4.96	3.90	2.36	3.64	1.35	3.44		
CHM-derived height (m)	2.96	5.65	3.71	4.85	4.68	4.04	2.70	3.78	1.69	3.30		
Error (m)	-0.18	0.39	-0.61	0.55	-0.28	0.14	0.34	0.14	0.34	-0.14	0.07	0.36

The height of sample trees extracted from CHM largely differed from ground measurement results because the handheld GPS failed to perform differential processing, which led to major positioning errors of approximately 10 m in general. The position of sample trees could not be accurately matched with CHM, and there was a large displacement. The canopy height widely varied, showing significant discrepancy. Consequently, the error of CHM could not be accurately determined.

Dynamic extent

In 2015, the area of the mangrove patch was 8.16 ha (Fig. 2a). With an average annual growth rate of 3.7%, the patch area increased to 8.79 ha by October 2017 (Fig. 2a), accounting for an increase of 7.9%.

From 2015 to 2017, an area of 81,540 m^2 in the patch remained stable. Nevertheless, the patch expanded by 6,356 m^2 and shrunk by 19 m^2 (Fig. 2c).

Due to the limitation imposed by the seawall, most of the patch expansions were sea-oriented (Fig. 2c, Fig. 3a1 and Fig. 3a2), and the maximum distance of expansion was 24 m (Fig. 3a3). The only exception is a landward extension of 89 m^2 at the north-west end, filling the gap between the mangrove patch and the seawall. As no artificial afforestation was implemented in the study area, the process of patch expansion was natural. The patch expansion mainly occurred in the eastern part below the central part of the patch, and the expansion in northwestern part of the patch was very small. One possible explanation was that the water of the Naso River in the northern part of the study area and the ocean current during the ebb tide were affected by the branches and leaves of mangroves as they flow through the mangroves forest in the northwest of the patch. Blocked by stem and breathing roots, river and ocean currents were slowed down (Kathiresan 2003; Kathiresan and Rajendran 2005; Swales et al. 2007; Ong and Gong 2013). Sediment carried by rivers and ocean currents formed fine sand deposits in the southeastern part of the patch, resulting in rapid flattening of seafloor topography. This scenario created favorable conditions for the expansion of mangroves (de Boer 2002).

During the field investigation, local residents were found to collect *Concha ostreae* and raise ducks in the mangrove patch, but no evidence of artificial afforestation or other destructive human activities (such as clearing mangroves to build shrimp ponds) was found through image interpretation and field investigation. Therefore, the expansion and shrinkage of the patch occurred naturally. In other words, the death of the mangrove forest and destruction of the mangrove habitat were not attributable to human interference. The possible cause of shrinkage is the death of trees due to pests and diseases, as shown in Figs. 3b1, 3b2 and 3b3.

Spatial pattern of canopy height of patches and its evolution

CHM and d-CHM of the patch in 2015 and 2017 are shown in Fig. 4a1, Fig. 4b1, and Fig. 4c1, respectively. Their local 3D views are shown in Fig. 4a2, Fig. 4b2, and Fig. 4c2, respectively. UAV remote sensing exhibited a clear advantage over traditional field investigation. The conventional field investigation provided only a limited number of sample tree height, whereas UAV remote sensing provided patch CHM and d-CHM at a resolution of 1 m × 1 m. In addition to the stepless amplification and 3D view mentioned above, UAV remote sensing could also be used for canopy height classification and many other applications. It intuitively reflected the whole landscape of the patch and the distribution of the tree height in each section at the local scale.

In Fig. 4a1 and 4b1, the canopy height of each section of the patch appear to widely vary irrespective of the year (2017 or 2015). The canopy was higher in the northwestern section than in the southeastern section. Applying the spatial statistical method, the CHM of the two years was counted. The average height of the patch canopy was 2.8 m in 2015 and 3.4 m in 2017, as shown in Table 2.

Table 2
Statistics of crown height in 2015 and 2017

Year	Item	Total	0.1-1.0 m	1.1-2.0 m	2.1-3.0 m	3.1-4.0 m	4.1-5.0 m	5.1 m-	Mean (m)
2015	area (m^2)	82588	461	16139	27683	30893	7367	45	2.8
	%	100.0	0.6	19.5	33.5	37.4	8.9	0.1	
2017	area (m^2)	88856	126	23497	6584	23797	30058	4794	3.4
	%	100.0	0.1	26.4	7.4	26.8	33.8	5.4	

It can be seen from Table 2 that there is a great difference in canopy height in the two years, which is reflected in the large difference in area percentage of each height class, especially in the two height classs of 2.01–3.00 m and 4.01–5.00 m.

From Fig. 4c1, it could be concluded that the canopy height of patches increased generally from 2015 to 2017, with decrease in some areas. Canopy height increases of more than 1.0 m accounted for a large area, and those more than 1.5 m accounted for a small area, with a maximum increase of up to 3.2 m. Figure 4c1 shows that 88.2% of the patch area experienced canopy height increase, while 11.8% of the patch area experienced

canopy height decrease from 2015 to 2017. Canopy height increased by more than 0.5 m in 70.9% of the patch area, and by more than 1.0 m in 38.9% of the patch area increased. In contrast, it decreased by more than 0.5 m in 5.0% of the patch area, as shown in Table 3.

Table 3
Changes in crown height

Range of change (m)	Total	-3.2–1.5	-1.5–1.0	-1.1–0.5	-0.5–0.0	0.0-0.5	0.5-1.0	1.1–1.5	1.5–3.2	Mean (m)
Area (m^2)	88855	932	1031	2490	6069	15369	28432	19743	14789	0.78
%	100.0	1.0	1.2	2.8	6.8	17.3	32.0	22.2	16.6	

In the GIS software environment, six vertical profiles (a1 to a6, distance between each profile line was 90 m to 130 m) were set up from northwest to southeast. These profiles were basically perpendicular to the seawall; three horizontal profiles (b1 to b3, at distances of 19 m, 43 m, and 72 m, respectively, from the seawall) were also generated and they were basically parallel to the seawall. In each vertical and horizontal profile line, 100 evenly located sample points were set. The heights of all 100 sample points in the CHM of 2015 and 2017 were extracted and the canopy height curve of each section is shown in Fig.5.

Figure 5a1–5a6 show that the canopy height exhibited a decreasing trend from inside (near the seawalls) to outside (to the seaward) longitudinally (perpendicular to seawall) in both 2015 and 2017. The height of trees was higher near the seawall than in offshore areas. This trend was not as clear in profile line a6 as it was close to a culture pond in the southeast (Fig. 2a and 2b). This trend is different from that of a mangrove patch in the West Alligator River in northern Australia, where the mangroves in the middle section were higher than those seaward and landward (Lucas et al. 2002). Horizontally (parallel to the seawall), the canopy height on the landward side (Fig. 5b1, about 19 m from the seawall) and the seaward side (Fig. 5b3, about 72 m from the seawall) showed a decreasing trend from the northwest to the southeast in both years. In other words, the trees were higher in the northwest and lower in the southeast. However, this regularity was not obvious in the middle of the patch (Fig. 5b2).

Figures 4c1 and 5a1–5a6 show that, in general, the canopy height increase from 2015 to 2017 was slightly higher in mangroves on the seaward side than those on the landward side. Nevertheless, this trend was not obvious. The increase of canopy height was similar in some areas (Fig. 5a4), but it widely varied in most areas (Fig. 5a2, 5a3 and 5a5). In some areas, the canopy height increase of mangroves on the seawall side was greater than those on the seaward side (Fig. 5a3 and Fig. 5a6). In other sections, the canopy height increase on the seaward side was larger than that on the seawall side (Fig. 5A1 and Fig. 5a5). Longitudinally, the canopy height increase exhibited a strong regularity. The crown height increase during 2015–2017 was more than 1 m in most areas from 210–360 m and in some areas from 415–475 m to the northwest of the patch and in some areas from 10–70 m to the southeast of the patch, and also the newly formed mangrove, especially along the middle profile line (Fig. 5b2). The decrease in canopy height did not exhibit any spatial regularity. Canopy height decreased in many areas of the patch, with a maximum decrease of 3.1 m. In addition, there was no linear relationship between canopy height increase during 2015–2017 and that in 2015.

The regular distribution of canopy height increase in the patch might be related to the time of the formation of the mangrove patch and the nutrient content of the bottom soil. The following possible explanations are proposed: 1) The patch was originally on an open beach. After the seawall was built in 1969, the Naso River and ocean currents were slowed down by the seawall, during which sediment deposition began in front of the seawall. This led to the gradual rise in the seafloor. After the seafloor was elevated above the average sea level, a large number of drifting propagule (Hypocotyl of *Avicennia marina* mainly) from the Naso River and ocean currents began to take root, settled, and grew in front of the seawall. As a result, the mangroves first formed in front of the seawall, and then gradually spread seaward (Li and Zhou 2017). The height of the canopy in the coastal area is higher than that of those on the seaward side. 2) Likewise, the mangrove formation time in the northwest section near the Naso River estuary was earlier than that in the southeast section. Consequently, the height of the tree canopy was higher in the northwest section and slightly shorter in the southeast.

The main reason for the decrease in canopy height might be the death of forest due to pest infestation. Regional pest disasters frequently occur in the study site and its surrounding areas due to the marine pollution and disappearance of large area primary vegetation in the adjacent coastal zone, which were replaced with Eucalyptus plantation, and other factors. The mangroves of this path were damaged by *Hyblaea puera* in September and October 2015, and was seriously damaged by *Oligochroa cantonella* in May 2016 (Fan and Wang 2017), and about 80% of the leaves were found to be eaten during the field work in August 2016. From afar, the mangrove forest appeared yellow in color (Li and Zhou 2017). During field investigation for sample trees in October 2017, about one-third of the trees were found to be dead in some areas, leaving large gaps in the mangrove forest. By comparing the two temporal DOM, it can be found that the forest in the patch was very prosperous in 2015 (Fig. 6a), but by 2017, due to the death of a considerable number of trees in the middle of the patch, the dead trunks were clearly visible on the image, and many gaps with a diameter of more than 5 m appeared (Fig. 6b), resulting in a significant decrease in the canopy height (Fig. 6c).

The increase of canopy height was the result of mangrove forest growth. As shown in Fig. 7, the tree density increased in 2017 and the tidal channels became smaller, compared to those in 2015.

According to the remote sensing images, the trees were thriving in most area in 2015 and 2017, but the increase of canopy height was so high that it is difficult to establish a specific and reasonable explanation. Possible reasons are as follows: 1) During the monitoring period, some area had soil rich in nutrients, promoting the growth rate of trees above the normal level. 2) In October 2017, the wind speed was high during UAV photo acquisition. The wind might have blown the branches upwards, increasing the apparent height of the tress. It is noteworthy that the mangrove habitat is in great danger, and the growth of mangroves is slow. Therefore, further study and analysis are required to fully understand the actual cause of the increase.

Discussion

In general, meter-scale resolution satellite images, such as SPOT5, IKONOS, China ZY-3, and GF-1/2 have been used for monitoring and mapping mangrove forests on the local level (Wang et al. 2004; Proisy et al. 2007; Kanniah et al. 2007; Vo et al. 2013; Rizki et al. 2017; Liu et al. 2017). Some studies have also used sub-meter-resolution satellite images, such as Quick Bird and WorldView-2 (Kux et al 2012; Wang et al. 2014; Heenkenda et al. 2014), and the aerial photography (Manson et al. 2001, 2003; Sulong et al. 2002; Dahdouh-Guebas et al.

2002, 2004; Benfield et al. 2005). China is located in the northern margin of mangrove vegetations. With a general heigh below 4 m and slow growth, most mangrove forests exist as shrubbery. A previous study showed that the average height of a seven-year-old *Avicennia marina* plantation was only 1.20 m, and the crown size was only 1.75 m × 1.73 m. The average height of an eight-year-old *Rhizophora stylosa* plantation was only 1.80 m, and the crown size was only 1.15 m × 1.11 m (Liao et al. 1996). Therefore, the meter-level resolution of satellite remote sensing images is not suitable for mapping young mangrove forests (Zhou et al. 2016, 2018). In this particular research area, the crown diameter of most newly formed mangrove forests has been found to be only about 1 m, which is attributable to the short period of monitoring. Digital orthophoto images with resolution up to 0.1 m × 0.1 m have incomparable advantages over other remote sensing images for short-term monitoring of changes in mangrove patches, especially for annual monitoring.

Traditional field investigations (sample plots or sample tree measurement) will only provide information about the height of trees in a very small area (usually 100–900 m^2) or at a point (a sample tree). As mangroves are usually distributed in muddy tidal zones, where walking is very difficult, the measurement of field sample plots or trees is extremely strenuous. Consequently, only a limited number of sample plots or sample trees can be considered, which poses a significant challenge to the development of a canopy height model that can accurately reflect the height distribution of forest patches. On the contrary, it is easier to generate high-precision DEM, DSM, and CHM using UAV imagery. With a scale of 1 m × 1 m, CHM comprehensively reflects the height of trees in patches in great detail. d-CHM derived from these models reflects changes in the height of forest patches during the monitoring period and provides detailed information for mangrove and coastal zone protection and management

In this study, the elevation accuracy of CHM and d-CHM in two years are both very high, and the error can be ignored for mangrove height measurement. The data quality was highly reliable, and the patch d-CHM was objective and reflected changes in tree heights accurately. However, the slowly growing shrubbery of *Avicennia marina* community in the patch could not be satisfactorily explained. According to data, from 2015 to 2017, the canopy height increased by more than 1 m in more than 1/3 of the area and by more than 1.5 m in 16.6% of the area, with a maximum increase of 3.2 m (Table 2 and Fig. 4). It is difficult to offer a reasonable explanation based on existing knowledge. Therefore, so it is necessary to investigate this scenario more deeply. Specifically, more accurate sample tree surveys, involving the accurate determination of the exact position of the sample trees (the plane error should be less than 1 m) and measurement of their growth rate, need to be conducted.

Conclusion

In 2015 and 2017, an approximately rectangular mangrove patch with an area of 8.8 ha was monitored via UAV remote sensing. Two annual digital orthophoto maps with resolution of 0.1 × 0.1 m were acquired. The average deviation of images from the two phases was 0.63 m and the maximum deviation was 0.75 m, which satisfied the requirement of annual dynamic analysis of the patch. The resolution of DEM and DSM was 1 m × 1 m, and the average error of the height of 10 sample trees extracted from CHM in 2017 and measured results on the ground was 0.09 m. The average error of d-CHM was − 0.004 m and the maximum error was − 0.050 m. It could be concluded that CHM and d-CHM were suitable for the annual dynamic analysis of mangrove canopy height.

From 2015 to 2017, the area of the mangrove patch increased from 8.16 ha to 8.79 ha, with an average annual increase of 3.7%. The patch expanded by 6356 m^2, shrunk by 19 m^2, and expanded 24 m into the sea. The driving factors were the natural processes of mangrove growth. The canopy height distribution exhibited a strong regularity; the height of the canopy decreased from northwest to southeast in the transverse direction (parallel to the seawall) and from the land side to the sea side in the longitudinal direction (vertical to the seawall). From 2015 to 2017, the canopy height increased in 88.2% of the patch area, with a maximum increase of 3.2 m. In contrast, the canopy height decreased in 1.8% of the patch area, with a maximum decrease of 3.1 m. The increase could be attributed to the natural growth of trees and the decrease to severe insect damage. However, further investigation is required to verify the reasons. Nevertheless, the DOM, CHM, and d-CHM obtained through UAV remote sensing reflected the condition of the patch and its overall changing trend not only at the regional scale, but also at the local scale with high precision. UAV remote sensing exhibits an incomparable advantage over traditional methods for studying the spatial variability of mangrove forests, which would contribute towards the conservation and management of mangrove forests.

Declarations

Conflict of interest

The authors declare that they have no conflicts of interest.

Acknowledgements

We promise that the study was performed according to the international, national and institutional rules considering biodiversity rights. And we extend our thanks to Mr. Bo Su from Beilunhe National Natural Reserve in Guangxi, China and Mr. Shishang Li from Forestry Bureau of Fangchenggang City of Guangxi of China for their helpful in our field investigation. This research was founded by the Asia-Pacific Network for Sustainable Forest Management and Rehabilitation (APFNet).

References

1. Aslan A, Rahman AF, Warren MW, Robeson SM (2016) Mapping spatial distribution and biomass of coastal wetland vegetation in Indonesian Papua by combining active and passive remotely sensed data. Remote Sens Environ 183:65–81. doi:10.1016/j.rse.2016.04.026
2. Benfield SL, Guzman HM, Mair JM (2005) Temporal mangrove dynamics in relation to coastal development in Pacific Panama. J Environ Manage 76:263–276. doi:10.1016/j.jenvman.2005.02.004
3. Benzeev R, Hutchinson N, Friess DA (2017) Quantifying fisheries ecosystem services of mangroves and tropical artificial urban shorelines. Hydrobiologia 803(1):225–237. doi:10.1007/s10750-017-3299-8
4. Blasco F, Saenger P, Janodet E (1996) Mangroves as indicators of coastal change. Catena 27(3):167–178. doi:10.1016/0341-8162(96)00013-6
5. Cao J, Leng W, Liu K, He Z, Zhu Y (2018) Object-based mangrove species classification using unmanned aerial vehicle hyperspectral images and digital surface models. Remote Sensing 10(1):89. doi:10.3390/rs10010089

6. Creation (2018) http://www.uav-china.com/page/default.asp?pageID=36. Accessed 05 May 2018 (in Chinese)
7. Dahdouh-Guebas F, Van Pottelbergh I, Kairo JG, Cannicci S, Koedam N (2004) Human-impacted mangroves in Gazi (Kenya): predicting future vegetation based on retrospective remote sensing, social surveys, and distribution of trees. Mar Ecol Prog Ser 272:77–92. doi:10.3354/meps272077
8. Dahdouh-Guebas F, Zetterström T, Rönnbäck P, Troell M, Wickramasinghe A, Koedam N (2002) Recent changes in land-use in the Pambala-Chilaw Lagoon complex (Sri Lanka) investigated using remote sensing and GIS: Conservation of mangroves vs. development of shrimp farming. Environ Dev Sustain 4(2):185–200. doi:10.1023/A:1020854413866
9. Dale PE, Chandica AL, Evans M (1996) Using image subtraction and classification to evaluate change in sub-tropical intertidal wetlands. Int J Remote Sens 17(4):703–719. doi:10.1080/01431169608949039
10. de Boer WF (2002) The rise and fall of the mangrove forests in Maputo Bay, Mozambique. Wetland Ecology Management 10(4):313–322. doi:10.1023/A:1020389420591
11. DJI-Innovation (2018) http://www.dji.com/cn/phantom-4, Accessed 31 Jeanery 2018 (in Chinese)
12. Doughty CL, Langley JA, Walker W, Feller IC, Schaub R, Chapman SK (2016) Mangrove range expansion rapidly increases coastal wetland carbon storage. Estuaries Coasts 39(2):385–396. doi:10.1007/s12237-015-9993-8
13. Duke N, Meynecke J-O, Dittmann S, Anger K (2007) A world without mangroves? *Science*. August, pp 41–42. doi:10.1126/science.317.5834.41b
14. Everitt JH, Escobar DE, Judd FW (1991) Evaluation of airborne video imagery for distinguishing black mangrove (*Avicennia germinans*) on the lower Texas Gulf Coast. J Coastal Res 7(4):1169–1173. doi:10.2307/4297936
15. Everitt JH, Yang C, Sriharan S, Judd FW (2008) Using high resolution satellite imagery to map black mangrove on the Texas Gulf Coast. J Coastal Res 24(6):1582–1586. doi:10.2112/07-0987.1
16. Fan HQ, Wang WQ (2017) Some thematic issue for mangrove conservation in China. *Journal of Xiamen University* (*Natural Science*)*Xiamen University Natural Science*, 56(3):323–330. (in Chinese). doi:10.6043/j.issn.0438-0479.201612003
17. FAO (2007) The world's mangroves 1980–2005. FAO Forestry Paper 153. FAO, Rome
18. Fatoyinbo TE, Simard M (2013) Height and biomass of mangrove in Africa from ICESat/GLAS and SRTM. *International Journal of Remote Sensing*, 2013, 34(1–2): 668–681. doi:10.1080/01431161.2012.712224
19. Fromard F, Vega C, Proisy C (2004) Half a century of dynamic coastal change affecting mangrove shorelines of French Guiana. A case study based on remote sensing data analyses and field surveys. Mar Geol 208(2–4):265–280. doi:10.1016/j.margeo.2004.04.018
20. Guo Q, Su Y, Hu T, Zhao X, Wu F, Li Y, Liu J, Chen L, Xu G, Lin G, Zheng Y, Lin Y, Mi X, Fei L, Wang X (2017) An integrated UAV-borne lidar system for 3D habitat mapping in three forest ecosystems across China. Int J Remote Sens 38(8–10):2954–2972. doi:10.1080/01431161.2017.1285083
21. Heenkenda M, Joyce K, Maier S, Bartolo R (2014) Mangrove species identification: Comparing WorldView-2 with aerial photographs. Remote Sensing 6(7):6064–6088. doi:10.3390/rs6076064

22. Kanniah KD, Wai NS, Shin AL, Rasib AW (2007) Per-pixel and sub-pixel classifications of high-resolution satellite data for mangrove species mapping. Applied GIS 3:1–22
23. Kathiresan K (2003) How do mangrove forests induce sedimentation? Revista De Biologia Tropical 51(2):355–360
24. Kathiresan K, Rajendran N (2005) Coastal mangrove forests mitigated tsunami. Estuarine Coastal Shelf Science 65(3):601–606. doi:10.1016/j.ecss.2005.06.022
25. Kovacs JM, Flores-Verdugo F, Wang J, Aspden LP (2004) Estimating leaf area index of a degraded mangrove forest using high spatial resolution satellite data. Aquat Bot 80(1):13–22. doi:10.1016/j.aquabot.2004.06.001
26. Kovacs JM, Wang J, Flores-Verdugo F (2005) Mapping mangrove leaf area index at the species level using IKONOS and LAI-2000 sensors for the Agua Brava Lagoon, Mexican Pacific. Estuaries Coasts Shelf Sci 62(1):377–384. doi:10.1016/j.ecss.2004.09.027
27. Kux HJH, Souza UDV (2012) Object-Based Image Analysis of WorldView-2 satellite data for the classification of mangrove areas in the city of SÃO LUÍS, MARANHÃO State, Brazil. *Electroencephalography & Clinical Neurophysiology*, I-4(6): 95–100. doi:10.5194/isprsannals-i-4-95-2012
28. Lee S-K, Fatoyinbo TE (2015) TanDEM-X Pol-InSAR inversion for mangrove canopy height estimation. *IEEE Journal of Selected Topics Appled Earth Observations and Remote Sensing*, 2015, 8(7): 3608–3618. doi:10.1109/JSTARS.2015.2431646
29. Lee T-M, Yeh H-C (2009) Applying remote sensing techniques to monitor shifting wetland vegetation: A case study of Danshui River estuary mangrove communities, Taiwan. Ecol Eng 35(4):487–496. doi:10.1016/j.ecoleng.2008.01.007
30. Li CG, Dai HB (2015) Two methods for measuring the changes in patch-number and area of mangrove driven by various factors through different ways. Acta Ecol Sin 35(6):1713–1726. doi:10.5846/stxb201305301247. (in Chinese).
31. Li CG, Liu SQ, Fan HQ, Dai HB (2012) A patch-based method for mechanism analysis on spatial dynamics of mangrove distribution. Acta Ecol Sin 32(14):4329–4342. doi:10.5846/stxb201106240935. (in Chinese).
32. Li CG, Zhou M (2017) Establishment and Expanding of Mangrove Forest After Construction of the Seawall —A Case Study of Tahji-Wanwei Seawall in Pear Bay. Guangxi Wetland science 15(1):1–9. Doi:10.13248/j.cnki.wetlandsci.2017.01.001. (in Chinese).
33. Li CG (2013) Research on the extraction of remote sensing information and mechanism of spatial dynamic of mangrove forest. *Beijing: Science press*. 113–140pp. (in Chinese)
34. Li SH, Li GC (1993) Chinese survey of China Bays (Vol.12). *Beijing: China ocean press*. 268-310pp. (in Chinese)
35. Liao BW, Zheng DJ, Zheng SF (1996) Present situation and prospect of mangrove afforestation in south China coast. *Protection Forest Science and Technology*, 1996, 29(4): 30–34. (in Chinese)
36. Liu M, Li H, Li L, Man W, Jia M, Wang Z, Lu C (2017) Monitoring the Invasion of spartina alterniflora using multi-source high-resolution imagery in the Zhangjiang Estuary, China. Remote Senings 9(6):539. doi:10.3390/rs9060539
37. Lovelock CE, Cahoon DR, Friess DA, Guntenspergen GR, Krauss KW, Reef R, Rogers K, Saunders ML, Sidik F, Swales A, Saintilan N, Thuyen AX, Triet T (2015) The vulnerability of Indo Pacific mangrove forests to sea-

level rise. Nature 526:559–563. doi:10.1038/nature15538

38. Lucas RM, Ellison JC, Mitchell A, Donnelly B, Finlayson M, Milne AK (2002) Use of stereo aerial photography for quantifying changes in the extent and height of mangroves in tropical Australia. Wetlands Ecol Manage 10(2):161–175. doi:10.1023/A:1016547214434
39. Manson FJ, Loneragan NR, McLeod IM, Kenyon RA (2001) Assessing techniques for estimating the extent of mangroves: topographic maps, aerial photographs and Landsat TM images. Marine Freshwater Research 52(5):787–792. doi:10.1071/MF00052
40. Manson FJ, Loneragan NR, Phinn SR (2003) Spatial and temporal variation in distribution of mangroves in Moreton Bay, subtropical Australia: A comparison of pattern metrics and change detection analyses based on aerial photographs. Estuar Coast Shelf Sci 57(4):653–666. doi:10.1016/S0272-7714(02)00405-5
41. Nagalakshmi R (2017) Mangrove restoration map preparation using remote sensing and GIS. Ecology Environment Conservation 23(2):1219–1224
42. Neukermans G, Dahdouh-Guebas F, Kairo JG, Koedam N (2008) Mangrove species and stand mapping in Gazi Bay (Kenya) using Quickbird satellite imagery. Journal Spatial Science 53(1):75–86. DOI:10.1080/14498596.2008.9635137
43. Olwig MF, Sørensen MK, Rasmussen MS, Danielsen F, Selvam V, Hansen LB, Nyborg L, Vestergaard KB, Parish F, Karunagaran VM (2007) Using remote sensing to assess the protective role of coastal woody vegetation against tsunami waves. Int J Remote Sens 28(13–14):3153–3169. doi:10.1080/01431160701420597
44. Ong JE, Gong WK (2013) Structure, function and management of mangrove ecosystems. In: ISME Mangrove Educational Book Series No. 2. International Society for Mangrove Ecosystems (ISME), Okinawa, Japan, and international Tropical Timber Organization (ITTO). Yokohama, Japan, p 43
45. Otero V, Kerchove RVD, Satyanarayana B, Martínez-Espinosa C, Fiso MAB, Ibrahim MRB, Sulong I, Mohd-Lokman H (2018) Managing mangrove forests from the sky: Forest inventory using field data and unmanned aerial vehicle (UAV) imagery in the Matang mangrove forest reserve, peninsular Malaysia. For Ecol Manage 411:35–45. doi:10.1016/j.foreco.2017.12.049
46. Palacios ML, Cantera JR (2017) Mangrove timber use as an ecosystem service in Colombian Pacific. Hydrobiologia 803:345–358. doi:10.1007/s10750-017-3309-x
47. Proisy C, Couteron P, Fromard F (2007) Predicting and mapping mangrove biomass from canopy grain analysis using Fourier-based textural ordination of IKONOS images. Remote Sens Environ 109(3):379–392. doi:10.1016/j.rse.2007.01.009
48. Rizki F, Situmorang ADL, Wau N, Lubis MZ, Anurogo W (2017) Mapping of vegetation and mangrove distribution level in Batam island using SPOT-5 satellite imagery. Journal of Geoscience Engineering Environment Technology 2(4):264–267. doi:10.24273/jgeet.2017.2.4.1002
49. Rodriguez W, Feller IC (2004) Mangrove landscape characterization and change in Twin Cays, Belize using aerial photography and IKONOS satellite data. Atoll Res Bull 513:1–22. doi:10.24273/jgeet.2017.2.4.1002
50. Saenger P, Hegerl EJ, Davie JDS (1983) Global status of mangrove ecosystems. Commission on Ecology Papers No. 3. Gland, Switzerland. World Conservation Union (IUCN)
51. Saleh MA (2007) Mangrove vegetation on Abu Minqar island of the Red Sea. Int J Remote Sens 28(23):5191–5194. doi:10.1080/01431160500391932

52. Simard M, Rivera-Monroy VH, Mancera-Pineda JE, Castaneda-Moya E, Twilley RR (2008) A systematic method for 3D mapping of mangrove forest based on Shuttle Radar Topography Mission elevation data, ICEsat/GLAS waveforms and fields data: Application to Ciénaga Grande de Santa Marta, Colombia. Remote Sens Environ 112(5):2131–2144. doi:10.1016/j.rse.2007.10.012
53. Simard M, Zhang K, Rivera-Monroy VH, Ross MS, Ruiz PL, Castaneda-Moya E, Twilley RR, Rodrihuez E (2006) Mapping height and biomass of mangrove forests in Everglades national park with SRTM elevation data. Photogrammetric Engineering Remote Sensing 72(3):299–311. doi:10.14358/PERS.72.3.299
54. Sulong I, Mohd-Lokman H, Mohd-Tarmizi K, Ismail A (2002) Mangrove mapping using Landsat imagery and aerial photographs: Kemaman District, Terengganu, Malaysia. Environment Development Sustainability 4(2):135–152. doi:10.1023/A:1020844620215
55. Swales A, Bentley S, Lovelock C, Bell R (2007) Sediment processes and mangrove-habitat expansion on a rapidly- prograding muddy coast, New Zealand. Proceedings of the Sixth International Symposium on Coastal Engineering and Science of Coastal Sediment Processes, New Orleans, USA, May 2007. *Coastal Sediments*, 2: 1441–1454. doi:10.1061/40926(239)111
56. Teh SY, Koh HK, Liu P, L-F, Md.Ismaila Al, Lee HL (2009) Analytical and numerical simulation of tsunami mitigation by mangroves in Penang, Malaysia. J Asian Earth Sci 36(1):38–46. doi:10.1016/j.jseaes.2008.09.007
57. Tian J, Wang L, Li X, Gong H, Shi C, Zhong R (2017) Comparison of UAV and WorldView-2 imagery for mapping leaf area index of mangrove forest. International Journal Applied Earth Observations Geoinformation 61:22–31. doi:10.1016/j.jag.2017.05.002
58. UNEP (2014) The Importance of Mangroves to People: a Call to Action. United Nations Environment Programme Programmer
59. Vo QT, Oppelt N, Leinenkugel P, Kuenzer C (2013) Remote sensing in mapping ecosystem——An object-based approach. Remote Sensing 5(1):183–201. doi:10.3390/rs5010183
60. Walters BB, Rönnbäck P, Kovacs JM, Crona B, Hussain SA, Badola R, Primavera JH, Barbier E, Dahdouh-Guebas F (2008) Ethnobiology, socio-economics and management of mangrove forests: A review. Aquat Bot 89(2):220–236. doi:10.1016/j.aquabot.2008.02.009
61. Wang L, Sousa WP, Gong P (2004) Integration of object-based and pixel-based classification for mangrove mapping with IKONOS imagery. Int J Remote Sens 25(24):5655–5668. doi:10.1080/014311602331291215
62. Wang T, Zhang H, Lin H, Fang C (2014) Textural-Spectral Feature-Based Species Classification of Mangroves in Mai Po Nature Reserve from Worldview-3 Imagery. Remote Sensing 8(1):24. doi:10.3390/rs8010024
63. Yanagisawa H, Koshimura S, Goto K, Miyagi T, Imamura F, Ruangrassamee A, Tanavud C (2009) The reduction effects of mangrove forest on a tsunami based on field surveys at Pakarang Cape, Thailand and numerical analysis. Estuar Coast Shelf Sci 81(1):27–37. doi:10.1016/j.ecss.2008.10.001
64. Yanagisawa H, Koshimura S, Miyagi T, Imamura F (2010) Tsunami damage reduction performance of a mangrove forest in Banda Aceh, Indonesia inferred from field data and a numerical model. J Geophys Res Oceans, 115(C6) doi:10.1029/2009JC005587

65. Zhou M, Li CG, Dai HB (2016) Mapping of young mangrove forest by using remote sensing: A case study in the Maoweihai bay in Guangxi. Forest resources management, (6): 26–30. (in Chinese). doi:10.13466/j.cnki.lyzygl.2016.06.006
66. Zhou M, Li CG, Dai HB (2018) Factors influence the area accuracy of mangrove based on remote sensing and the measure need to be taken. Journal of Nanjing Forestry University (Natural Science Edition) 42(01):163–168. (in Chinese)

Figures

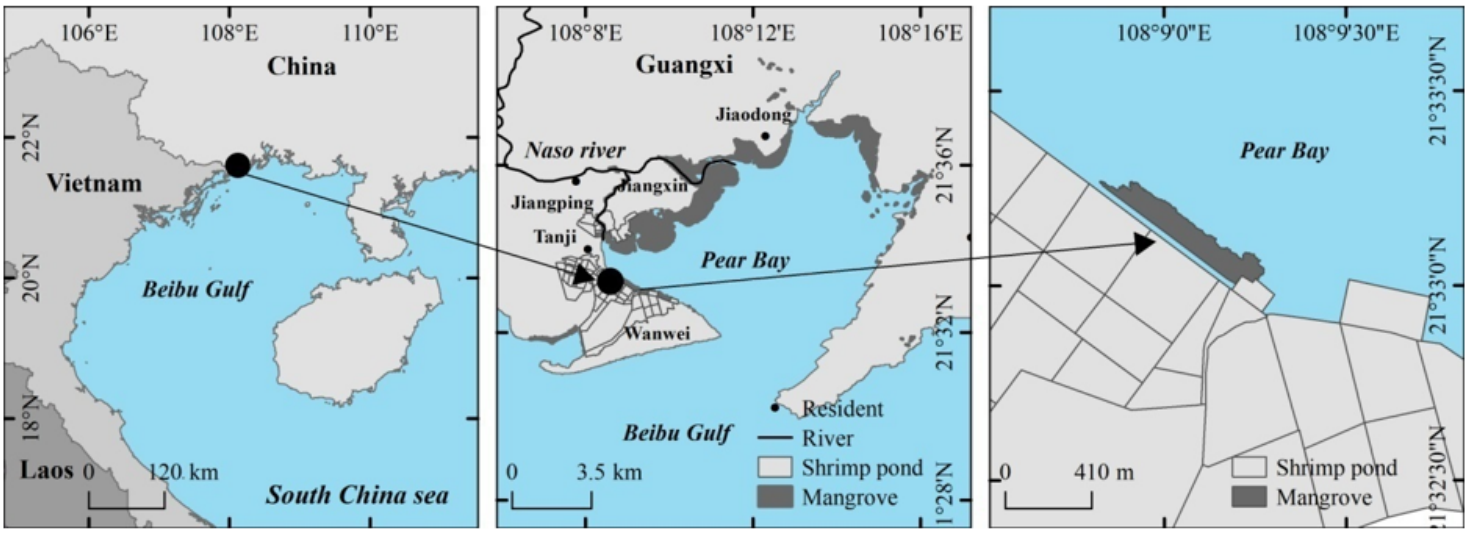

Figure 1

Location of the study site

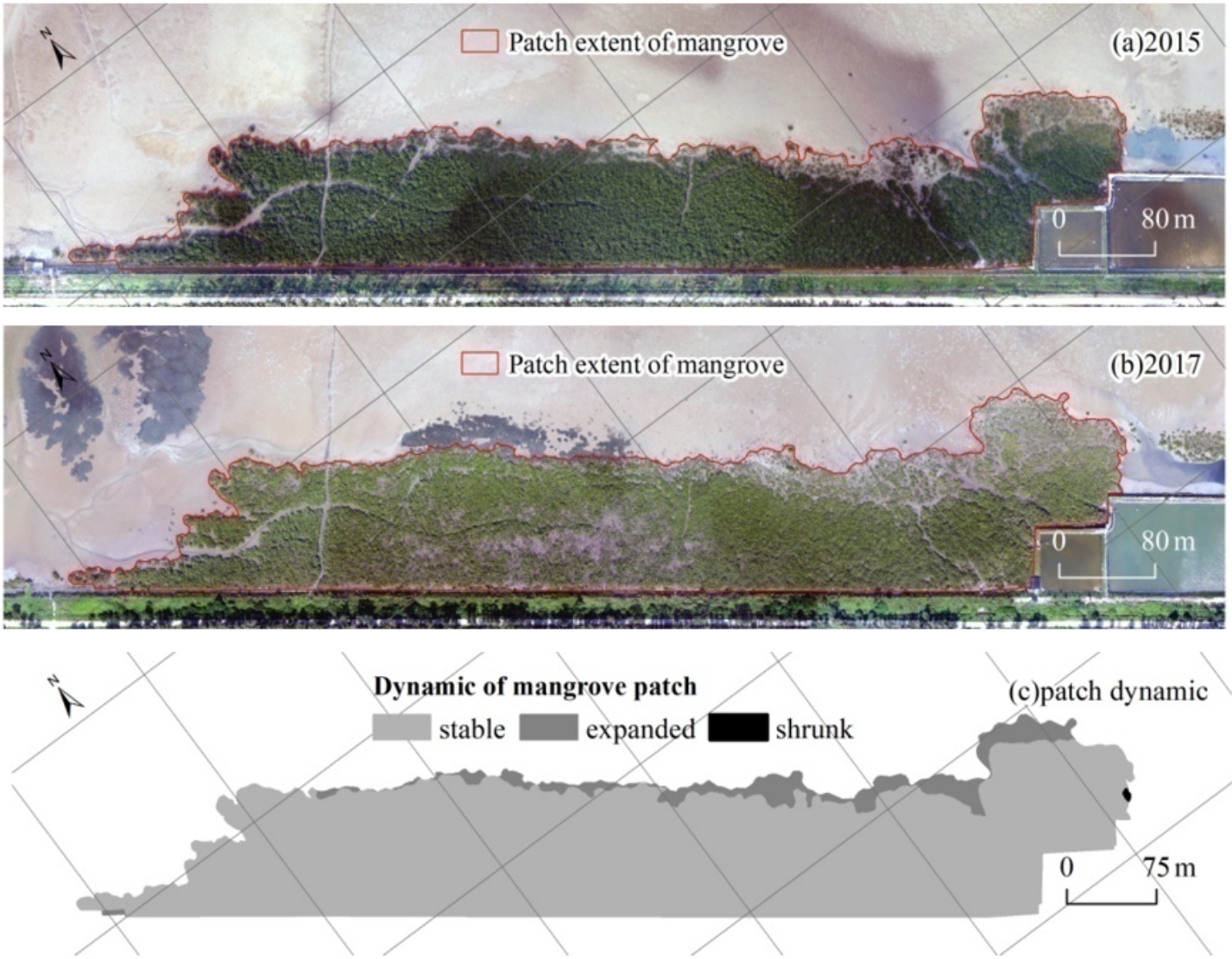

Figure 2

Patch extent and DOM of 2015 (a) and 2017 (b) and dynamic of the patch extent (c)

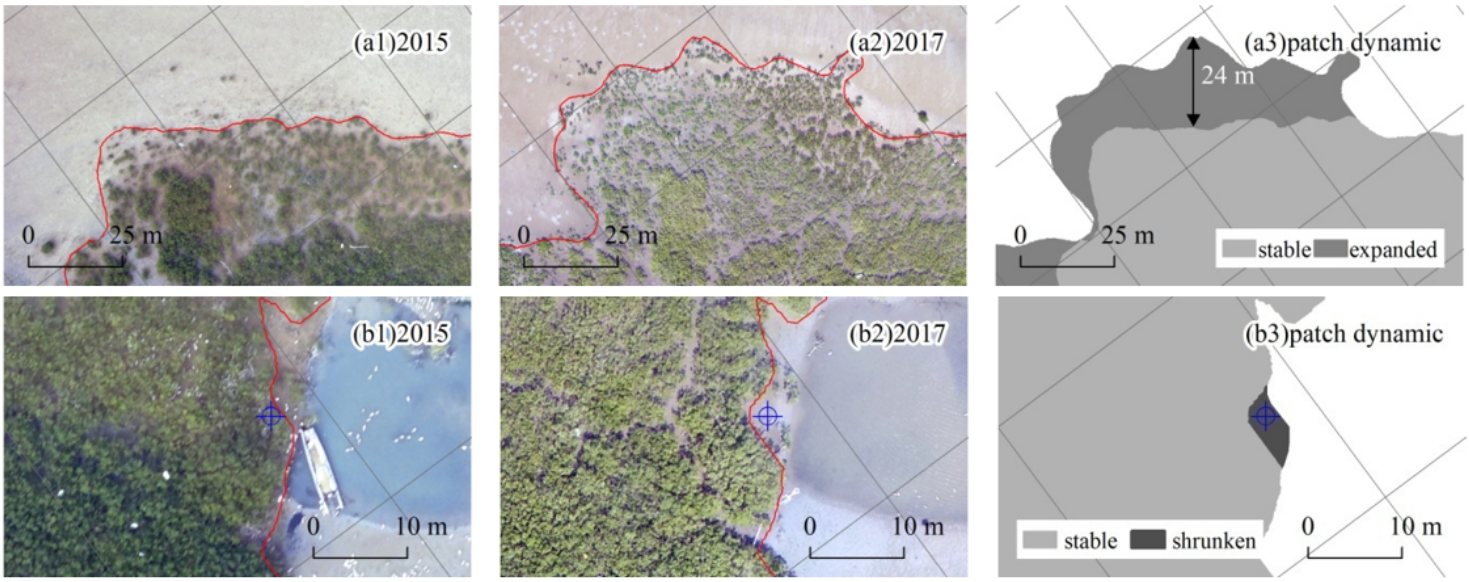

Figure 3

Patch expansion (a1, a2, a3) and shrinkage (b1, b2, b3) from 2015 to 2017

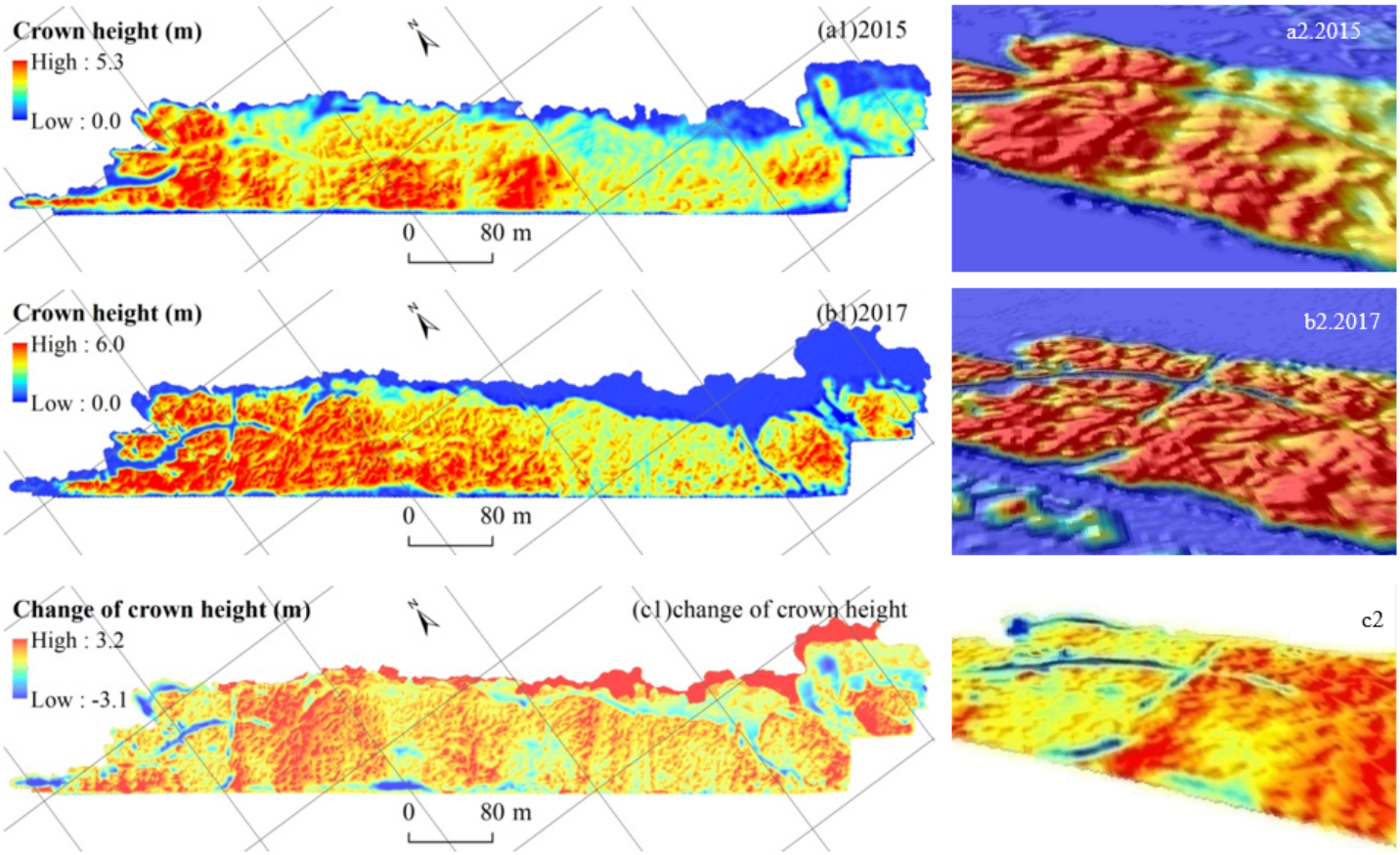

Figure 4

Patch CHM of 2015 (a1) and 2017 (b1) and its change map (c1) and their corresponding partial 3D views (a2, b2, c2)

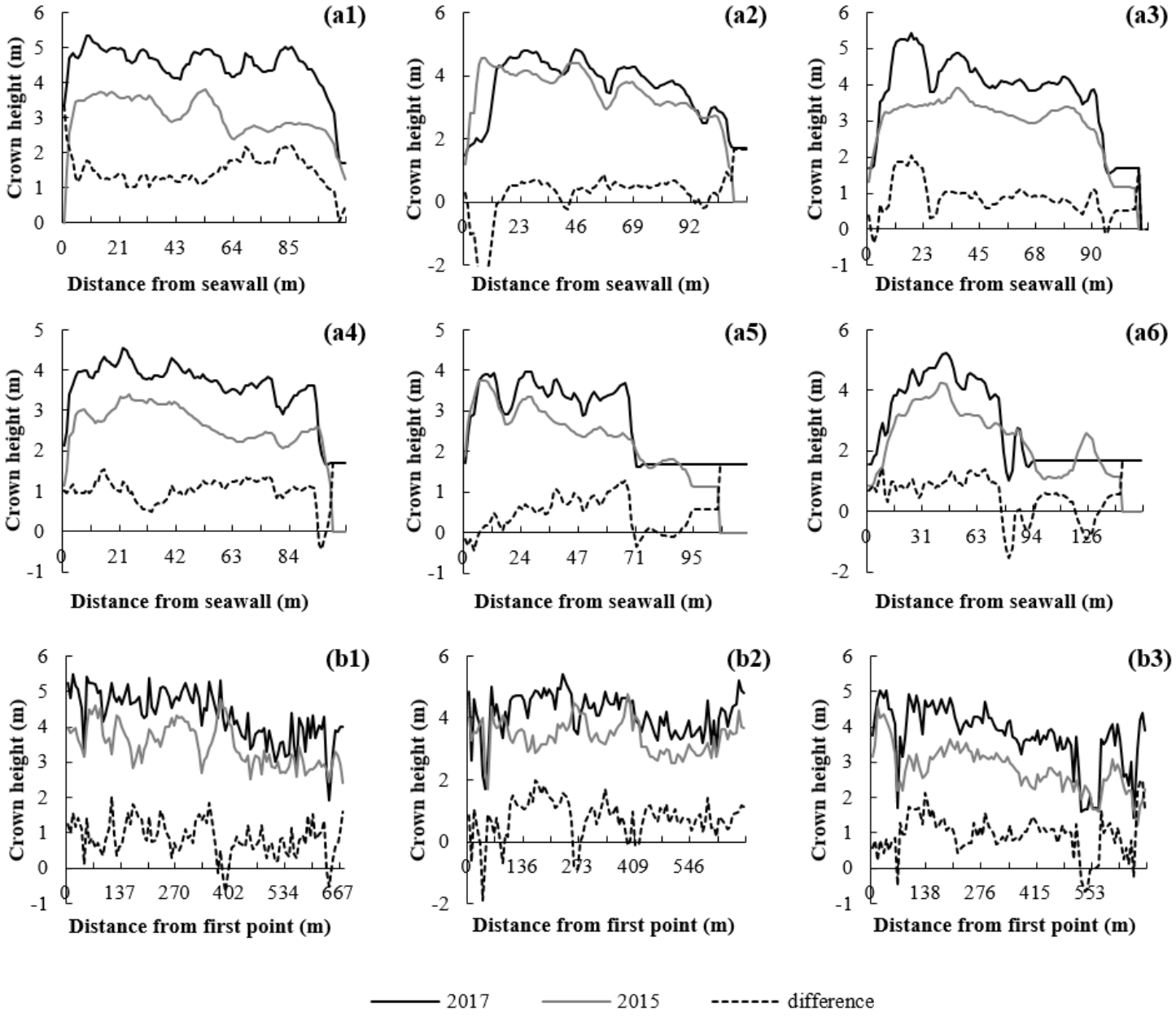

Figure 5

Comparison of CHM-derived heights for 2015 and 2017 along six section lines perpendicular to the seawall (a1-a6) and three section lines parallel to the seawall (b1-b3)

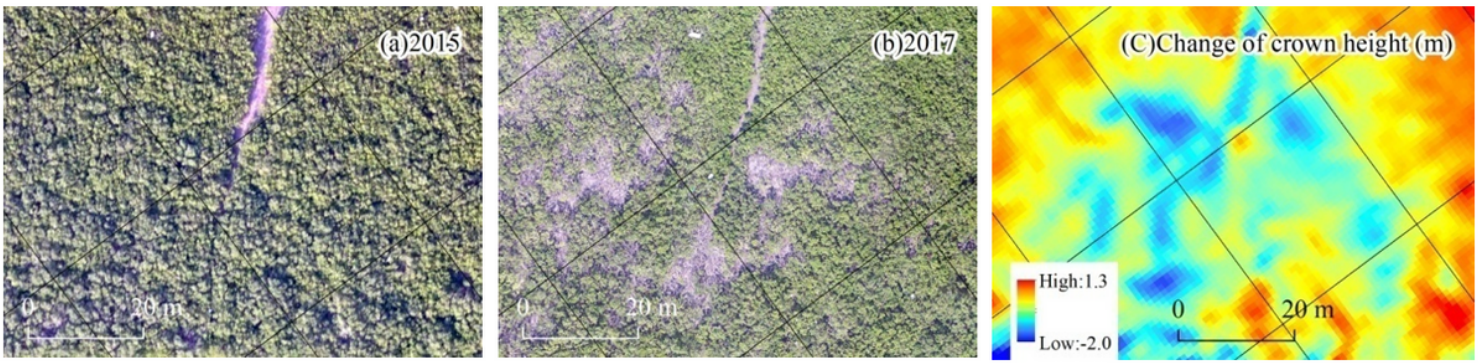

Figure 6

Reduction of crown height visible as gaps in the forest, attributable to the death of mangrove trees due to pest infestation

Figure 7

Crown height increase visible as high tree density